Ultrastructural distribution of presynaptic active zones and dense core vesicles in olfactory projection neurons of *Drosophila*

Abstract

In *Drosophila melanogaster*, olfactory projection neurons (PNs) convey odor information from peripheral olfactory center, antenna lobe, to central olfactory center, mushroom body (MB), and lateral horn (LH). In MB, the mechanisms underlining the transformation from coarse-coding PNs to sparse-coding MB intrinsic Kenyon cells (KCs) remain an open question. Here, we used HRP-labeled electron microscopy (EM) to volume reconstruct 89 PN axonal boutons in a reference area of the input region, the calyx of MB. The results showed that the number of presynaptic active zones (PAZs), neurotransmitter release site, is in positive linear correlation with the surface area of PN axonal boutons, while the number of dense core vesicles (DCVs), vesicles that containing neuropeptides, monoamines, or neurotrophic factors, is weakly related to the morphology of PN axonal boutons. Further analysis illustrated that DCVs preferentially exist in PN axonal boutons labeled by GH146-GAL4, a most widely used genetic marker for studying olfactory PNs. Our data suggest that synapses are uniformly distributed on the surface of all PN boutons, thus the neurotransmission capability of a PN axonal bouton could be predicted by its size, and PN subtypes release neuropeptides, monoamines, or neurotrophic factors, as well as classical neurotransmitters, to mediate the PN-KC transformation.

Keywords

olfactory projection neuron, mushroom body calyx, volume reconstruction, electron microscopy, presynaptic active zone, dense core vesicle, cluster.

Introduction

Environment information is sensed by peripheral sensory neurons and conveyed to central brain centers though various stages of neurons. Take odor information for example, odors were first sensed by olfactory sensory neurons in peripheral system and then conveyed to olfactory projection neurons, and then delivered to higher brain areas[1]. Besides classical neurotransmitters, neuropeptides, monoamines and neurotrophic factors play essential role in neurons communication in the central nervous system [2-5]. How neurons release these neural signal molecules to transmit information is a critical issue in neuroscience. Previous studies showed that before released, neurotransmitters are stored in small clear core vesicles that drifted or docked at PAZs, and neuropeptides, monoamines and neurotrophic factors are stored in large DCVs that drifted in neuron cytoplasm [6, 7]. It is reported that some neuropeptides serve as co-transmitter with neurotransmitter to modulate synaptic plasticity [8-11], which indicates that DCVs may be morphologically distributed at PAZs in axons. The questions that how DCVs distributed in

axons and their relationship with PAZs remain elusive.

The olfactory PNs of fruit fly provide us a convenient system to address these questions. In olfactory system of fly, PNs relay odor information from primary olfactory center, antenna lobe, to two central olfactory centers, mushroom body and lateral horn for modulating adaptive and innate behaviors [12]. Calyx is the input region of MB, where PNs transform coarse-coding odor information to sparse-coding odor information of MB KCs by forming a distinguishable structure called microglomerulus. It is reported that multiple mechanisms underline PN-KC transformation, including thresholding, input integration, sparse synaptic connection, developmental plasticity [13-16] etc., though no direct evidence showed that neuromodulators, neuropeptide, monoamine, or neurotrophic factors, mediate this process. It is reported that PNs release two types of neurotransmitters, acetylcholine or γ-aminobutyric acid (GABA) [17, 18]. Recent studies analyzed the transcriptome in PNs and identified neuropeptide-coding mRNA [19]. Previous EM results showed that some PN boutons contain DCVs[20]. These studies suggest that PNs release neuropeptide as co-transmitter.

Taking advantage of HRP-labeled EM volume reconstruction, we showed the distribution features of DCVs and PAZs in PN axonal boutons. We volume reconstructed 89 PN boutons in a reference region in MB calyx. According to the morphological parameters, these PN boutons are classified into 4 types: Normal Boutons, Thin Boutons, Unilobed Boutons, and Multi-branched Boutons. We found that the number of PAZs is linearly correlated with the surface area of boutons and the number of DCVs only shows a weak correlation with the volume of boutons. This pointed out that PAZs are uniformly distributed in all boutons while the distribution of DCVs is rarely correlated with bouton morphology. Comparing the density of DCVs in GH146 positive and GH146 negative boutons, we found that DCVs are enriched in GH146 positive boutons. Taken together, our results provided morphological evidence that synapses are uniformly distributed in all boutons and GH146 labeled PN subtypes release neuropeptide as co-transmitter.

Materials and methods

Fly strains

The y^1 w^{1118}; GH146-GAL4/CyO (Bloomington Drosophila Stock Center: 30026) was used to drive UAS-CD2::HRP/CyO (Bloomington Drosophila Stock Center: 8763).

EM sample preparation

EM sample preparation was performed as previously described [21] and modified by following procedure. Brains from female flies 4 days post-eclosion were dissected in 2.5% glutaraldehyde in 0.1 M Phosphate buffer (PB, PH at 7.4) on a cold plate at 4 □ and then fixed overnight at 4 □. After washing by 0.1 M TriHCl buffer (PH at 7.4) 3 times and each time for 10 minutes at 4 □, brains were stained by 1 mg/ml DAB in 0.1 M TriHCl (PH at 7.4) for 20 minutes at 4 □ and then transfer to room temperature

for 15 minutes. After washing by 0.1 M PB 3 times and each time for 10 minutes, brains were fixed with 1% OsO_4 in 0.1 M PB buffer for 2 hours at 4 □. After washing by double distilled water 3 times and each time for 10 minutes, brains were stained with 2% Uranyl acetate overnight at 4 □. Dehydration and infiltration with resin were performed following standard protocols [22].

EM data acquisition

The EM sample was trimmed and oriented vertically with the MB calyx at the top. Serial EM images were acquired by focused ion beam scanning electron microscopy (FIB-SEM, Helios Nanolab 600i). The EM sample was imaged in x and y with 5 nm pixels in a small region of 20 μm × 20 μm in the center of MB calyx. Meanwhile, a focused beam of 30 kV gallium atoms was used to mill EM sample every 40 nm to acquire a raw dataset of 658 slices.

Statistical methods

The cable length, N end points, volume, and average smoothed surface area (AVGs surface area) were withdrawn from Fiji-TrakEM2 and named as skeleton length, end points, volume, and surface area. PAZs and DCVs were annotated and withdrawn by customed dissector function in Fiji-TrakEM2. All data were tested for normal distribution by Kolmogorov-Smirnov test. Unpaired t-test and one-way ANOVA were used to compare the difference between two groups and multiple groups, respectively. For correlation analysis, Spearman correlation coefficients for the skeleton length and the number of segment, and Pearson correlation coefficients for the volume and the surface area, the volume and the number of DCVs, and the surface area and the number of PAZs. Different models were used to obtain a high cluster quality, the Akaike information criterion for morphology cluster and Bayesian information criterion for PAZ-DCV cluster[23, 24].

Results

Volume reconstruction of PNs in a reference region of MB calyx

As the second relay, Olfactory PNs connect antenna lobe with MB calyx and LH (Figure 1 A). MB calyx is a circle from posterior view under EM, and it is surrounded by KC cell bodies and PN processes (Figure 1 B). In MB calyx, A microglomerulus is composed by large presynaptic PN axonal boutons, numerous tiny postsynaptic dendritic claws, and some other MB extrinsic neurons ([17],Figure1 D). For quantitively analyzing the DCVs and PAZs in PN axonal boutons, we used FIB-SEM to collect a serial EM dataset in volume of 20 μm × 20 μm × 25 μm in the center of the MB calyx, and the resolution in xy axis and z axis are 5 nm and 40 nm respectively (Figure1 C).

PN boutons were identified in individual EM section by four distinct features: 1) large section area; 2) enriched clear core vesicles; 3) multiple PAZ sites and 4) large mitochondria inside. We manually connected the center of the same PN bouton in consecutive sections to draw its skeleton (Figure 1 D). The skeletons provide the length of a bouton major axis and the branch

number of a bouton. And then we volume reconstructed PN boutons to depict their shapes, by which we can calculate the volume and surface area of a bouton (Figure 1 D). Under EM, most PAZs in insects like *Drosophila* or *locust* display an electron dense ribbon called T-bar and DCVs were large electron dense dots[6, 25]. Accordingly, we annotated the PAZs and DCVs (Figure 1D). To increase the accuracy for the quantitative analysis of PAZs and DCVs, PN boutons that partially extended out of the EM dataset were not reconstructed (Figure S1). PN processes barely contain vesicles, mitochondria, or synapses, which suggests that the function is unrelated to information transformation between neurons, therefore, PN processes were not reconstructed (Figure S1).

Eventually, we reconstructed 89 PN boutons in total, and found that they are uniformly spread in the EM dataset, and are variable in size and shape. We found that most of PN boutons are in parallel with the z-axis of the dataset (Figure 1E).

Classification of PN boutons according to EM volume parameters

To address the distribution of the DCVs and PAZs in fine structure of PN boutons, we analyzed 4 morphological parameters of the reconstructed PN boutons: skeleton length, number of end points, volume, and surface area in Fiji-TrakEM2. The skeletons of PN boutons provided 2-dimensional (2D) morphological parameters, the skeleton length, the length of the major axis of a PN bouton, and the end points, the branch number of a PN bouton (see Methods, Figure 2A). Most of PN boutons (80/89) have 2-8 end points (1-7 branch sites) with a mean of about 5, and their skeleton lengths varied from 3 μm to 23 μm with a mean of 16.9 μm (Figure S2). Considering the effect of the branch sites in PN skeletons, we calculated the segment number (N_seg) of a bouton in equation：

$$N_{seg} = 2(N_{end} - 1) - 1$$

, so that the cable from an ending to a branch site and between 2 adjacent branch sites were taken as a segment (Figure 2A). We found that the skeleton length of PN boutons is positively related to the segment number (Figure 2B). This result indicates that the mean segment length (L_seg) of PN boutons, which equaled the skeleton length divided by N_seg, is similar. Besides the skeleton differences, The sizes of PN boutons are variable. Therefore, we analyzed the volume and surface area of PN boutons (see Methods). The surface area of most PN boutons is from 10 μm² to 90 μm², with an average of 43.47 μm² and the volume of PN boutons ranges from 1.3 μm³ to 39.9 μm³, with an average of 12.35 μm³, and 80% of them (72/90) are between 10-30 μm³ (Figure S2). The volume and surface area of PN boutons were also positively correlated, which indicates that the fineness or relative diameter of PN boutons is homologous (Figure 2D). The surface area/volume ratio (S/V ratio) was calculated to represent the fineness of a PN bouton, and the bigger the S/V ratio is, the thinner the PN bouton is.

Previous study defined 3 distinct patterns of PN boutons under light microscopy: unilobed PN boutons, clustered PN boutons and elongated PN boutons, and 2 separable patterns under electron microscopy: short segments and long slender axons[20].

After collecting all the beforementioned morphological parameters, we classified the 89 reconstructed PN boutons by automatic clustering. According to N_seg, L_seg, and S/V ratio, PN boutons were automatically clustered into 4 clusters by Akaike information criterion-based two-step clustering (Figure 2 E): The biggest cluster of PN boutons (51/89) have about 6 segments, 3 μm segment length and 3.4 μm^{-1} S/V ratio, and show no obvious morphological features. Thus, we named them Normal Bouton; The cluster of 11 PN boutons that contains about 20 segments and 2 μm segment length were named as Multi-branched Bouton; The cluster of 13 PN boutons that has about 1 segment and about 10 μm segment length were named as Unilobed Boutons; The cluster of 14 boutons that owns about 3 segments, 3 μm segment length ,and the biggest S/V ratio, 4.6 μm^{-1} , were named as Thin Bouton (Figure 2 E and F). Therefore, we found that there are 4 kinds of morphological distinct PN boutons by unbiased cluster.

Ultrastructural distribution of PAZs and DCVs in PN boutons

In the central nervous system of *Drosophila*, most PAZs are characterized by an electron dense ribbon, T-bar, while some PAZs show non-ribbon but attached by an adjunct postsynaptic density (PSD) (Figure 3A-C). As mentioned above, the neuropeptide-containing DCVs are electron-denser and larger than transmitter-contained clear core vesicles (Figure 3A-C). Following the distinct criterions of PAZs and DCVs, we annotated all PAZs and DCVs in our volume reconstructed 89 PN boutons. In subcellular level, we found that besides drifted in PN boutons, DCVs often distributed in 3 sites: close to membrane (Figure 3A), close to PAZ (Figure 3B), and close to mitochondria (Figure 3C). DCVs close to non-PAZ membrane and PAZs are corresponding to extra-synaptic and synaptic releasing of neuropeptide respectively, while few reports pointed that DCVs are related to mitochondria. The histogram of DCVs showed that PN boutons contains about 19 DCVs on average, with maximum of 50 and minimum of 1 (Figure S2). The histogram of PAZs showed that PN boutons contains about 44 PAZs on average,, with maximum of 126 and minimum of 9 (Figure S2). To test the distribution relationship of PAZs and DCVs with the morphology of PN boutons, we analyzed the correlation between the number of DCVs and the volume, and the number of PAZs and the surface area of PN boutons, respectively, as the DCVs drift inside boutons and PAZs are attached to bouton membrane. The results showed that PAZs are positively related to bouton surface area, while DCVs are weakly related to bouton volume (Figure 3D and E). These results indicate that PAZs are uniformly distributed on the membrane in all boutons and DCVs distribution is weakly related to the morphology of PN boutons. Next, we compared the difference of PAZ number and DCV number in 4 types of morphological clustered boutons. The DCV number is almost even among 4 types of boutons, except for Multi-branched boutons contain more DCVs than the Unilobed boutons and Thin boutons (Figure 4F). The DCV number is significant different among 3 kinds of morphological distinct boutons (the Normal boutons show no difference from others). These results, together with the correlation results, demonstrate that the morphology or size of PN boutons determine the PAZs

inside, while the DCV distribution is unrelated to PN morphology.

DCVs preferentially exist in GH146 positive boutons

To analyze the distribution relationship between PAZs and DCVs in PN boutons, we used Bayesian information criterion-based two-step cluster to classify PN boutons according to the PAZ number and DCV number inside. We found that the boutons are optimally clustered into 3 groups: 27 boutons contain less PAZs and DCVs were clustered as low PAZ low DCV (lPAZ-lDCV) boutons; 35 boutons contain more PAZs and DCVs were clustered as high PAZ high DCV (hPAZ-hDCV) boutons; 27 boutons contain more PAZs but less DCVs were clustered as high PAZ low DCV (hPAZ-lDCV) boutons (Figure 4A). Considering that the PAZ number are closely related to the surface area of boutons (Figure 3E), it could be conjectured that small bouton contains less PAZs and less DCVs, and during bouton enlargement, it raises two situations: in some boutons, both PAZs and DCVs are accumulated, while in other boutons, only PAZs are accumulated and DCVs remain unchanged during bouton enlargement. Thus we hypothesized that the distribution of DCVs may be relate to genetically different PN subtypes. Previous sequencing studies showed that PN subtypes labeled by *abnormal chemosensory jump 6 (acj6)* strongly express sNPF gene and PN subtypes labeled by *ventral veins lacking (vvl)* express neuropeptide Tachykinin gene [19]. The acj6 and vvl are expressed in anterodorsal PNs and lateral PNs exclusively in PNs that labeled by GH146-GAL4 lines, a most widely used GAL-4 lines to study PNs [26, 27]. We expressed UAS-mCD8::horseradish peroxidase (HRP) in GH146-GAL4, by which the membrane of GH146 positive boutons are electron-denser than that of GH146 negative boutons under EM ([28], Figure 4 B and C). We compared the distribution difference of PAZs and DCVs between GH146 positive and GH146 negative boutons. The results showed that most GH146 positive boutons are hPAZ-hDCV boutons with a few exceptions, and the GH146 negative boutons are either lPAZ-lDCV boutons or hPAZ-lDCV boutons (Figure 4 A and D). Statistical analysis showed that the DCV number and DCV density in GH146 positive boutons are significantly higher than that of GH146 negative boutons, while there is no difference between GH146 positive and GH146 negative boutons in PAZ number and PAZ density. To summarize, these results indicate that DCV distribution is related to genetically different PN subtypes while PAZs are not.

Discussion

In this study, we volume reconstructed 89 PN boutons in a reference region in mushroom body calyx of Drosophila and revealed some distribution features of DCVs and neurotransmitter releasing site, PAZs. The morphological parameter-based cluster results demonstrated that a small portion of PN boutons show distinct morphology under EM, include Multi-branched Boutons, Unilobed Boutons, and Thin Boutons, while most PN boutons seem to be alike. In subcellular level, the results showed that the DCVs exist in 4 patterns including drifted in cytoplasm, close to mitochondria or T-bar, or membrane, and the PAZs are uniformly distributed on the surface of all boutons in a density of 1 PAZ per square microns. By the comparison of

PAZs and DCVs between GH146 positive and GH146 negative boutons, we found that GH146 positive boutons contain significantly higher density DCVs than GH146 negative boutons, while the PAZs inside show no difference between them. The discussion focus on the developmental implication of morphological distinct boutons and the distribution characteristics of PAZs and DCVs in boutons.

Axons exhibit activity-dependent structural plasticity during development and in mature brains.

Morphological distinct PN boutons

Olfactory PNs convey odor information from antenna lobe to mushroom body KCs by forming microglomeruli, a distinct structure that is centered by a large PN boutons and surrounded by numerous tiny KC claws and some other MB extrinsic neuropiles, such as anterior paired lateral (APL) and dopaminergic neurons [29-31]. Previous studies showed that PN boutons in MB calyx distribute in a stereotypy pattern and perform no subregion preference [32]. Under light microscopy, it is found that PN boutons appear to display 3 patterns: unilobed, elongated, and clustered [20]. Our study showed that under electron microscopy, PN boutons are classified into 4 types according to its fine morphological parameters. Obviously, the Multi-branched Boutons are related to the clustered boutons under light microscopy, and they are large in volume and surface area (figure 2E and [20]). Unilobed Boutons we identified are morphologically like elongated boutons under light microscopy, as they own a long skeleton length and extend no branches, and the unilobed boutons under light microscopy are related to the Thin Boutons under EM, as they both display small branches, small skeleton length and thin diameter (large S/V ratio). Most PN boutons show no characteristics in morphological parameters, so that cannot be clearly clustered. It appears that most of the Normal Boutons are like unilobed or elongated boutons under light microscopy, as they are small in volume and extend a few short branches. Axons undergo remodeling during development and in mature brains, including axon branching and pruning[33-35]. We proposed that 4 kinds of morphologically distinct boutons can mutually transformed, in a way that Thin Boutons and Unilobed Boutons become Multi-branched Boutons by axon branching, and Multi-branched Boutons become Thin Boutons and Unilobed Boutons by axon pruning.

Distribution characteristics of PAZs in PN boutons

It is widely accepted that neurotransmitters are stored in clear core vesicles (CCVs) and released into synaptic cleft though PAZs [36, 37]. In *Drosophila*, most PAZs are featured by an electron-dense ribbon called T-bar, except for a handful number of non-ribbons PAZs [20, 25]. The correlation between PAZs and CCVs makes it reasonable to estimate the capability of a bouton to release neurotransmitter by its PAZ number. Our results showed that the number of PAZs is closely related to the volume and surface area of a bouton, which indicates that PAZs are uniformly distributed in all PN boutons, with a density of 1 PAZ per micron (Figure 3E). Therefore, the larger bouton is, the more PAZs it contains. Our results is consistent with previous studied

that PAZ density is controlled both in neuron muscular junction (NMJ) and central nervous system (CNS) [38].Assuming that all PAZs are of even probability to releasing neurotransmitter, the neurotransmission capability of PN boutons should be in corresponding to its volume (or surface area), thus the larger boutons have higher neurotransmission capacity. In *Drosophila*, it is found that prolonged deprivation of synaptic transmission from PNs or aging cause increasing bouton size and PAZ density [39, 40]. Unlike our definition of PAZ density, the number of PAZ per square microns, the PAZ density in these studies is calculated by the number of PAZ in individual bouton. We take the hypothesis that the PAZ number per square microns is the key determinant of the efficiency of boutons to transmit information, and it is controlled by unknown mechanisms[38]. On chronic or aged condition, as the releasing capability or probability of individual synapse decreased, flies take a compensate strategy to enlarge the bouton size and increase PAZ number to maintain its original PAZ density (PAZ per square microns). If it is true, what determines the PAZ density and what changes the PAZ density are of great importance deserve further explored.

Distribution characteristics of DCVs in PN boutons

Neuropeptide in *Drosophila* play key roles in regulation of physiological and behavioral roles, including development, feeding, growth, reproduction, and metabolism, and neuromodulation roles in olfaction, locomotor control and learning and memory [41-48].In olfactory pathway, it is proved that olfactory receptor neurons and mushroom body KCs release neuropeptide to facilitate and potentiate neurotransmission, respectively[10, 11]. Recent years, single cell sequencing results revealed that PN subtypes express neuropeptide-gene[19], and our results provide structure evidence that it is PN subtypes labeled by GH146-GAL4 that enrich in DCVs (Figure 4), thus it is of high possibility that PN subtypes labeled by GH146-GAL4 release neuropeptide as co-transmitter to modulate synaptic transmission between PNs and KCs. As a typical system for studying the transformation from coarse coding to sparse coding, multiple disciplines have been shown to underline PN-KC transformation, including thresholding, input integration, sparse synaptic connection, developmental plasticity [13-16], etc. Here, we propose that neuropeptide also participate in this process, as neuropeptide directly or indirectly modulate microcircuit[3]. Further functional studies could use GH146-GAL4 to explore what neuropeptide the PN release and its function in PN-KC neurotransmission. Unlike previous studies that a proportion of PN boutons only contain clear core vesicles[20], our results showed that all PN boutons contain DCVs, though a small number of PN boutons only contain a few DCVs (Figure 3D). This may be resulted from that some neuropeptides participate in axon guidance[49].

On the cellular level, Neuropeptide is packaged into DCVs in endoplasmic reticulum and transported to axons through trans-Golgi network and released at synaptic or extra-synaptic sites [50]. Our results showed that DCVs are distributed in 4 locations in bouton, including drifted in cytoplasm, close to PAZs, close to non-PAZ membrane (Figure 3A and B), and this result provide ultrastructural evidence for DCV transportation in fly brain. Notably, our results found that parts of DCVs in PN

boutons locate close to mitochondria (Figure 3C), and only a few reports in *C. elegans* found that neuropeptide releasing is related to mitochondria [51].One possibility is that DCVs and mitochondria are transport together through trans-Golgi network, and the other possibility is that these mitochondria-related DCVs are mitochondria-derived vesicles [50, 52].

In summary, we used HRP-labeled EM reconstruction to provide ultrastructural evidence that GH146 positive PN boutons release neuropeptide as co-transmitter and synapses are uniformly distributed in all PN boutons.

Reference

1. Leinwand, S.G. and S.H. Chalasani, *Olfactory networks: from sensation to perception.* Curr Opin Genet Dev, 2011. **21**(6): p. 806-11.
2. Hyman, S.E., *Neurotransmitters.* Curr Biol, 2005. **15**(5): p. R154-8.
3. Nusbaum, M.P. and D.M. Blitz, *Neuropeptide modulation of microcircuits*. Curr Opin Neurobiol, 2012. **22**(4): p. 592-601.
4. Heninger, G.R., P.L. Delgado, and D.S. Charney, *The revised monoamine theory of depression: a modulatory role for monoamines, based on new findings from monoamine depletion experiments in humans.* Pharmacopsychiatry, 1996. **29**(1): p. 2-11.
5. Skaper, S.D., *Neurotrophic Factors: An Overview.* Methods Mol Biol, 2018. **1727**: p. 1-17.
6. Gondre-Lewis, M.C., J.J. Park, and Y.P. Loh, *Cellular mechanisms for the biogenesis and transport of synaptic and dense-core vesicles.* Int Rev Cell Mol Biol, 2012. **299**: p. 27-115.
7. Kuznetsov, I.A. and A.V. Kuznetsov, *Chapter 13 - How Dense Core Vesicles Are Delivered to Axon Terminals â€“ A Review of Modeling Approaches*, in *Modeling of Microscale Transport in Biological Processes*, S.M. Becker, Editor. 2017, Academic Press. p. 335-352.
8. HÃ¶kfelt, T., et al., *Neuropeptide and Small Transmitter Coexistence: Fundamental Studies and Relevance to Mental Illness.* Front Neural Circuits, 2018. **12**: p. 106.
9. Nusbaum, M.P., D.M. Blitz, and E. Marder, *Functional consequences of neuropeptide and small-molecule co-transmission.* Nat Rev Neurosci, 2017. **18**(7): p. 389-403.
10. Root, C.M., et al., *Presynaptic facilitation by neuropeptide signaling mediates odor-driven food search.* Cell, 2011. **145**(1): p. 133-44.
11. Barnstedt, O., et al., *Memory-Relevant Mushroom Body Output Synapses Are Cholinergic.* Neuron, 2016. **89**(6): p. 1237-1247.
12. Masse, N.Y., G.C. Turner, and G.S. Jefferis, *Olfactory information processing in Drosophila*. Curr Biol, 2009. **19**(16): p. R700-13.
13. Turner, G.C., M. Bazhenov, and G. Laurent, *Olfactory representations by Drosophila mushroom body neurons.* J Neurophysiol, 2008. **99**(2): p. 734-46.
14. Li, H., et al., *Transformation of odor selectivity from projection neurons to single mushroom body neurons mapped with dual-color calcium imaging.* Proc Natl Acad Sci U S A, 2013. **110**(29): p. 12084-9.
15. Gruntman, E. and G.C. Turner, *Integration of the olfactory code across dendritic claws of single mushroom body neurons.* Nat Neurosci, 2013. **16**(12): p. 1821-9.
16. Elkahlah, N.A., et al., *Presynaptic developmental plasticity allows robust sparse wiring of the Drosophila mushroom body.* Elife, 2020. **9**.
17. Yasuyama, K., I.A. Meinertzhagen, and F.W. Schurmann, *Synaptic organization of the mushroom body calyx in Drosophila melanogaster.* J Comp Neurol, 2002. **445**(3): p. 211-26.
18. Liang, L., et al., *GABAergic Projection Neurons Route Selective Olfactory Inputs to Specific Higher-Order Neurons.* Neuron, 2013. **79**(5): p. 917-931.
19. Croset, V., C.D. Treiber, and S. Waddell, *Cellular diversity in the Drosophila midbrain revealed by single-cell transcriptomics.* Elife, 2018. **7**.
20. Butcher, N.J., et al., *Different classes of input and output neurons reveal new features in microglomeruli of the adult Drosophila mushroom body calyx.* J Comp Neurol, 2012. **520**(10): p. 2185-201.
21. Watts, R.J., et al., *Glia engulf degenerating axons during developmental axon pruning*. Curr Biol, 2004. **14**(8): p. 678-84.
22. Meinertzhagen, I.A., *Ultrastructure and quantification of synapses in the insect nervous system.* J Neurosci Methods, 1996. **69**(1): p. 59-73.

23. Schwarz, G., *Estimating the Dimension of a Model.* Annals of Statistics, 1978. **6**: p. 461-464.
24. Akaike, H., *A new look at the statistical model identification.* IEEE Transactions on Automatic Control, 1974. **19**(6): p. 716-723.
25. Wichmann, C. and S.J. Sigrist, *The active zone T-bar--a plasticity module?* J Neurogenet, 2010. **24**(3): p. 133-45.
26. Li, H., et al., *Classifying Drosophila Olfactory Projection Neuron Subtypes by Single-Cell RNA Sequencing.* Cell, 2017. **171**(5): p. 1206-1220 e22.
27. Lai, S.L., et al., *Clonal analysis of Drosophila antennal lobe neurons: diverse neuronal architectures in the lateral neuroblast lineage*. Development, 2008. **135**(17): p. 2883-93.
28. Schikorski, T., S.M. Young, Jr., and Y. Hu, *Horseradish peroxidase cDNA as a marker for electron microscopy in neurons*. J Neurosci Methods, 2007. **165**(2): p. 210-5.
29. Leiss, F., et al., *Synaptic organization in the adult Drosophila mushroom body calyx*. J Comp Neurol, 2009. **517**(6): p. 808-24.
30. Liu, X. and R.L. Davis, *The GABAergic anterior paired lateral neuron suppresses and is suppressed by olfactory learning.* Nat Neurosci, 2009. **12**(1): p. 53-9.
31. Mao, Z. and R.L. Davis, *Eight different types of dopaminergic neurons innervate the Drosophila mushroom body neuropil: anatomical and physiological heterogeneity.* Front Neural Circuits, 2009. **3**: p. 5.
32. Lin, H.H., et al., *A map of olfactory representation in the Drosophila mushroom body.* Cell, 2007. **128**(6): p. 1205-17.
33. Butz, M., F. Worgotter, and A. van Ooyen, *Activity-dependent structural plasticity.* Brain Res Rev, 2009. **60**(2): p. 287-305.
34. Jamann, N., M. Jordan, and M. Engelhardt, *Activity-dependent axonal plasticity in sensory systems.* Neuroscience, 2018. **368**: p. 268-282.
35. De Paola, V., et al., *Cell type-specific structural plasticity of axonal branches and boutons in the adult neocortex*. Neuron, 2006. **49**(6): p. 861-75.
36. Torrealba, F. and M.A. Carrasco, *A review on electron microscopy and neurotransmitter systems.* Brain Res Brain Res Rev, 2004. **47**(1-3): p. 5-17.
37. Vaithianathan, T., et al., *Nanoscale dynamics of synaptic vesicle trafficking and fusion at the presynaptic active zone.* Elife, 2016. **5**.
38. Clarke, G.L., J. Chen, and H. Nishimune, *Presynaptic Active Zone Density during Development and Synaptic Plasticity.* Front Mol Neurosci, 2012. **5**: p. 12.
39. Kremer, M.C., et al., *Structural long-term changes at mushroom body input synapses.* Curr Biol, 2010. **20**(21): p. 1938-44.
40. Pech, U., et al., *Optical dissection of experience-dependent pre- and postsynaptic plasticity in the Drosophila brain.* Cell Rep, 2015. **10**(12): p. 2083-95.
41. Nassel, D.R. and A.M. Winther, *Drosophila neuropeptides in regulation of physiology and behavior.* Prog Neurobiol, 2010. **92**(1): p. 42-104.
42. Riddiford, L.M., P. Cherbas, and J.W. Truman, *Ecdysone receptors and their biological actions.* Vitam Horm, 2000. **60**: p. 1-73.
43. Kim, S.K. and E.J. Rulifson, *Conserved mechanisms of glucose sensing and regulation by Drosophila corpora cardiaca cells.* Nature, 2004. **431**(7006): p. 316-20.
44. Shen, P. and H.N. Cai, *Drosophila neuropeptide F mediates integration of chemosensory stimulation and conditioning of the nervous system by food.* J Neurobiol, 2001. **47**(1): p. 16-25.
45. Isabel, G., et al., *AKH-producing neuroendocrine cell ablation decreases trehalose and induces behavioral changes in Drosophila.* Am J Physiol Regul Integr Comp Physiol, 2005. **288**(2): p. R531-8.
46. NÃ¤ssel, D.R., et al., *A large population of diverse neurons in the Drosophila central nervous system expresses short neuropeptide F, suggesting multiple distributed peptide functions.* BMC Neurosci, 2008. **9**: p. 90.
47. Winther, A.M. and R. Ignell, *Local peptidergic signaling in the antennal lobe shapes olfactory behavior.* Fly (Austin), 2010.

4(2): p. 167-71.

48. Krashes, M.J., et al., *A neural circuit mechanism integrating motivational state with memory expression in Drosophila.* Cell, 2009. **139**(2): p. 416-27.
49. HÃ¶kfelt, T., et al., *NPY and its involvement in axon guidance, neurogenesis, and feeding.* Nutrition, 2008. **24**(9): p. 860-8.
50. Zupanc, G.K., *Peptidergic transmission: from morphological correlates to functional implications.* Micron, 1996. **27**(1): p. 35-91.
51. Zhao, T., Y. Hao, and J.M. Kaplan, *Axonal Mitochondria Modulate Neuropeptide Secretion Through the Hypoxic Stress Response in Caenorhabditis elegans.* Genetics, 2018. **210**(1): p. 275-285.
52. Roberts, R.F., et al., *Defending the mitochondria: The pathways of mitophagy and mitochondrial-derived vesicles.* Int J Biochem Cell Biol, 2016. **79**: p. 427-436.

Figure 1. Volume reconstruction of PN boutons in a reference region of MB calyx.

(A) Schematic of olfactory projection neurons (PNs) in *Drosophila*. PNs convey odor information from antenna lobe (AL) to mushroom body (MB) and lateral horn (LH). The calyx (Ca) is the input region of MB. (B) Posterior view of Ca under electron microscopy (EM). (C) Raw dataset of photographs by focus ion beam serial electron microscopy (FIB-SEM) in the center of Ca in a volume of 20 μm × 20 μm × 20 μm. (D) Workflow of volume reconstruction of PN axonal boutons. Boutons on individual EM sections were identified by large area, multiple presynaptic active zones (PAZs) and with mitochondria and a great number of small clear core vesicles (CCVs) inside. The centers of boutons on consecutive sections were connected to draw the skeleton of boutons. Areas of boutons were depicted to draw the shape of boutons. PAZs and dense core vesicles (DCVs) were annotated in reconstructed boutons by blue dots and green dots, respectively. Scale bars, 5 μm. (E) Overall view of EM-reconstructed PN boutons.

Figure 2. Morphology characteristics of PN boutons.

(A) Skeletons of PN boutons show various numbers of end points (e) and branch site (b). (B) Considering the skeleton between two adjacent branch sites and an end point to the nearest branch site as a segment, the number of segments (N_seg) is positively related to the skeleton length of a bouton ($r = 0.90$). (C) Shapes of PN boutons show various size. (D) The volume if positively related to the surface area of a bouton ($r = 0.96$). (E) Cluster based on morphological parameters. 13 boutons with 1 segment and long segment length were clustered as Unilobed Boutons (yellow). 11 boutons with more than 10 segments were clustered as Multi-branched Boutons (pink). 14 boutons with largest surface area/volume (S/V) ratio were clustered as Thin Boutons (green). Boutons show no obvious features were clustered as Normal Boutons (blue). Scale bars in C and E are 5 μm.

Figure 3. Distribution of PAZs and DCVs in PN boutons.

(A-C) Subcellular distribution of PAZs (blue arrows) and DCVs (green arrows) in PN boutons. Most PAZs are featured by a T-bar ribbon (A and B) and a small number of PAZs are non-ribbon active zones (C). DCVs are varied in size and electron density (A and B). Besides drifted in boutons (A), DCVs are distributed in 3 patterns, close to membrane (A), close to T-bar (B), and close to mitochondria (Mi, C). Scale bars were 5 μm. (D) DCV number is weakly related to the volume of boutons ($r = 0.42$). (E) PAZ number is strongly related to the surface area of boutons ($r = 0.96$). (F) DCV number and PAZ number comparison among 4 kinds of morphological clustered boutons. Thin Boutons (green) contain least PAZs and DCVs, and Multi-branched Boutons (pink) contain the most PAZs and DCVs. (Unpaired t-test, * for $p < 0.05$, **** for $p < 0.0001$, n.s. for

no significance.)

Figure 4. DCVs preferentially exist in GH146 positive PN boutons.

(A) Cluster based on PAZ number and DCV number of PN boutons. The cluster of 35 boutons with more PAZs and DCVs was named as High PAZ High DCV boutons (H-PAZ; H-DCV, yellow). The cluster of 27 boutons with less PAZs and DCVs was named as Low PAZ Low DCV boutons (L-PAZ; L-DCV, green). The cluster of 27 boutons with more PAZs and less DCVs was named as High PAZ Low DCV boutons (H-PAZ; L-DCV, pink). (B) PAZs and DCVs in GH146 negative (GH146-) and GH146 positive (GH146+) boutons. Green arrows for DCVs and blue arrows for PAZs. Scale bars 5 μm. (C) GH146 positive membranes are electron denser than GH146 negative membranes. (D) The number of PAZs and DCVs in GH146 positive (dark) and GH146 negative boutons (gray). (E and F) The DCV number and DCV density of GH146 positive boutons are bigger than those of GH146 negative boutons, while the PAZ number and PAZ density show no difference between them. (Unpaired t-test, **** for $p < 0.0001$, n.s. for no significance.)

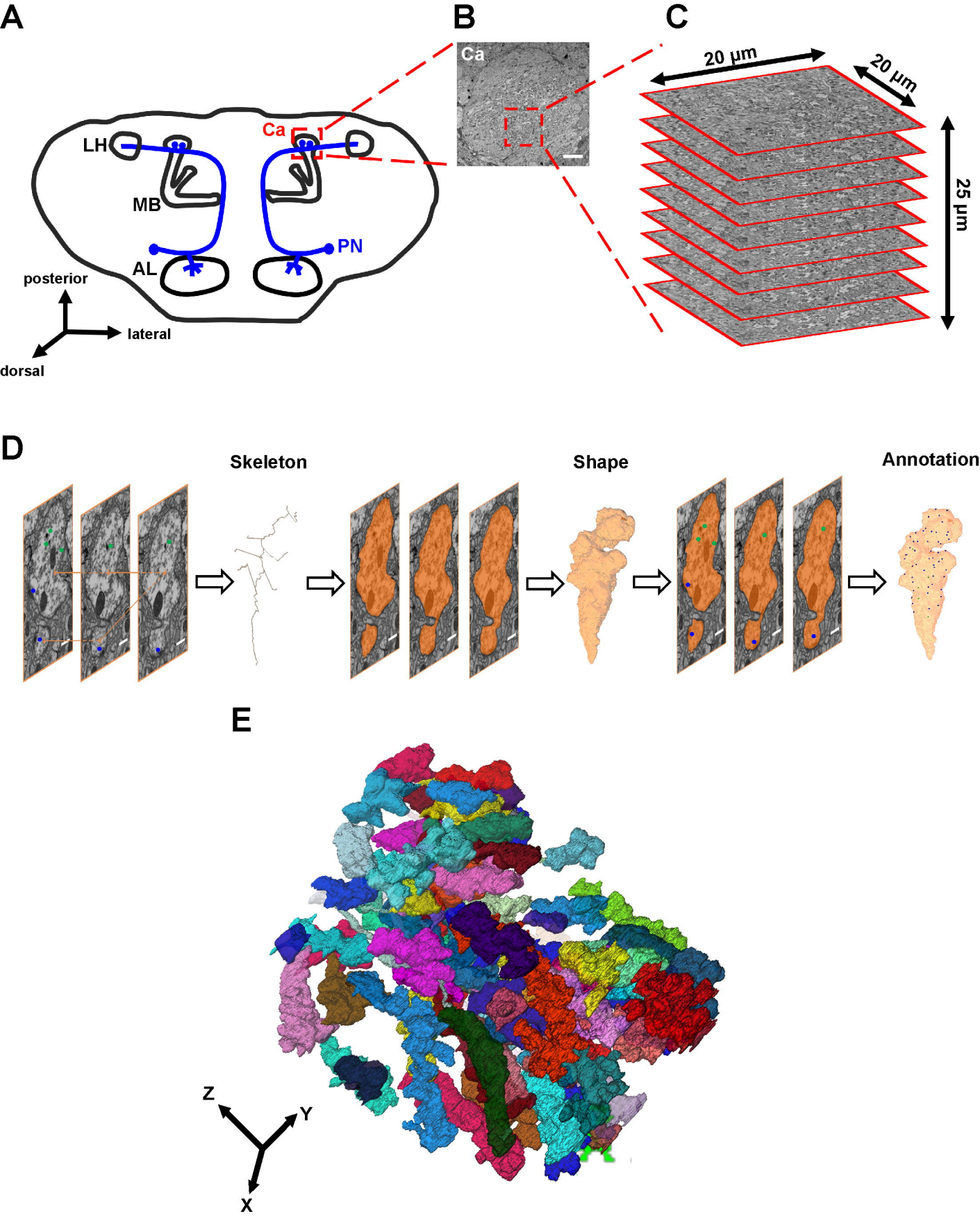
A
B
C
LH
MB
AL
PN
Ca
posterior
lateral
dorsal
Ca
20 µm
20 µm
25 µm
D
Skeleton
Shape
Annotation
E
Z
Y
X

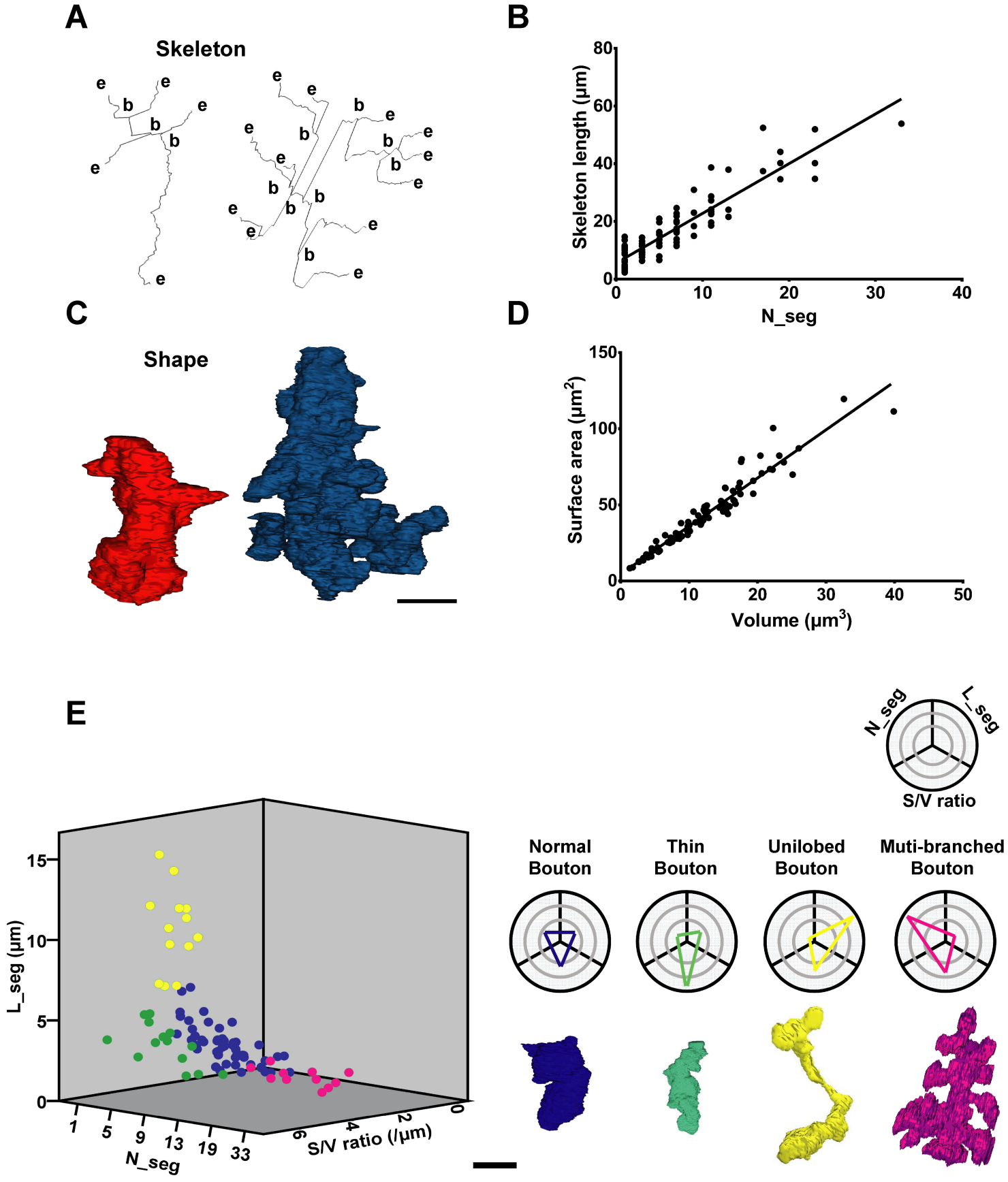
A
Skeleton
B
Skeleton length (μm)
N_seg
C
Shape
D
Surface area (μm²)
Volume (μm³)
E
N_seg
L_seg
S/V ratio
Normal Bouton
Thin Bouton
Unilobed Bouton
Muti-branched Bouton
L_seg (μm)
N_seg
S/V ratio (/μm)

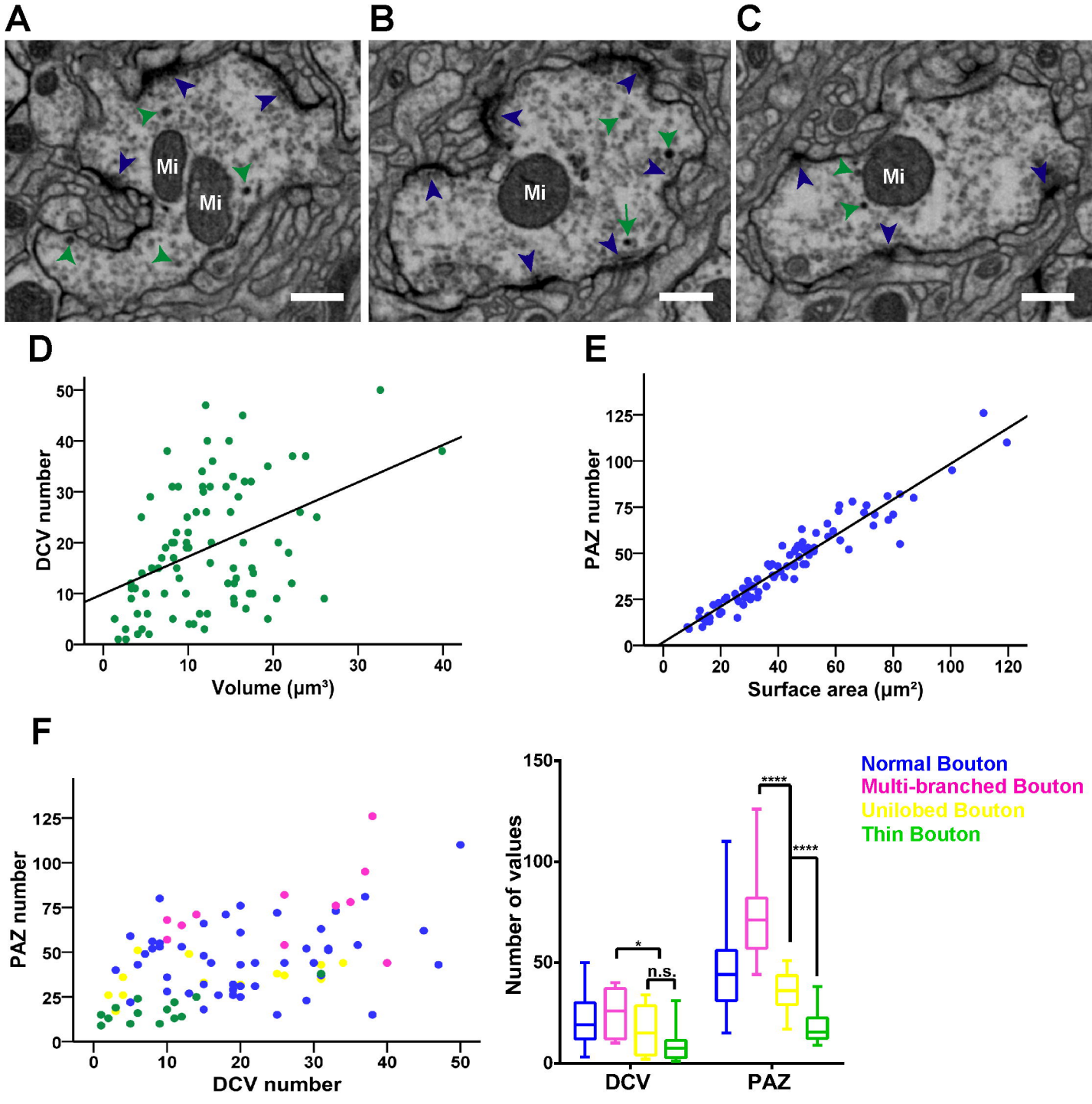
A
B
C
Mi
Mi
Mi
Mi
D
DCV number
Volume (μm³)
E
PAZ number
Surface area (μm²)
F
PAZ number
DCV number
Number of values
DCV
PAZ
*
n.s.
****
****
Normal Bouton
Multi-branched Bouton
Unilobed Bouton
Thin Bouton

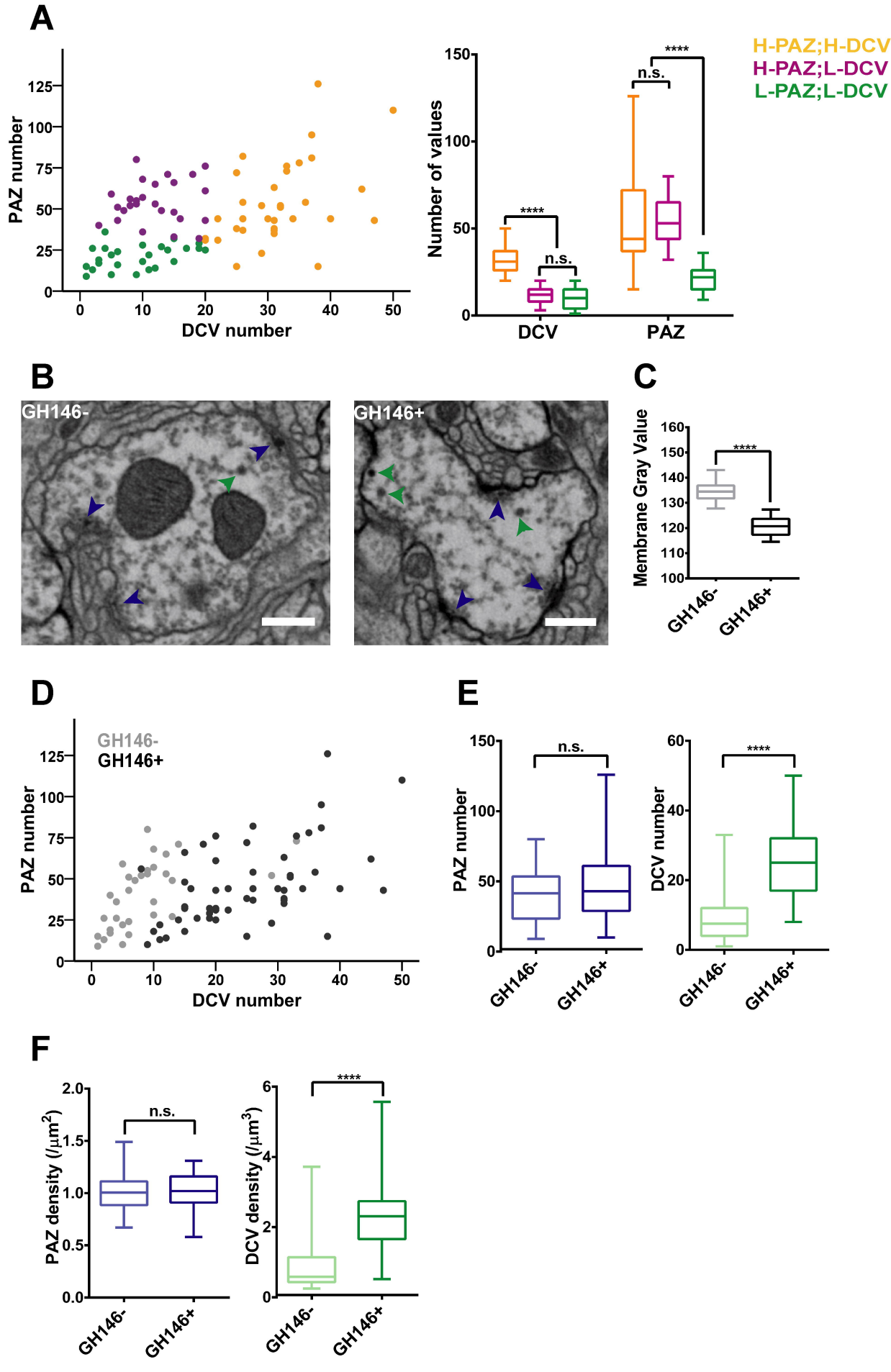
A
PAZ number
DCV number
Number of values
DCV
PAZ
n.s.
****
H-PAZ;H-DCV
H-PAZ;L-DCV
L-PAZ;L-DCV
B
GH146-
GH146+
C
Membrane Gray Value
GH146-
GH146+
D
GH146-
GH146+
PAZ number
DCV number
E
PAZ number
DCV number
n.s.
****
F
PAZ density (/μm²)
DCV density (/μm³)
n.s.
****
GH146-
GH146+